First estimate of the NA62 sensitivity to the rare decay $K^+ \to \mu^+ \nu_\mu X$, $X \to \gamma\gamma$

Rebecca Murta

September 30, 2020

Abstract

Light, weakly coupled new particles with couplings to muons have been proposed which could resolve the discrepancy between measured and predicted values for the anomalous magnetic moment of the muon. They may also act as dark matter mediators. A muonphilic scalar particle X may be produced in rare kaon decays and could be observed by NA62. In this project, the branching ratio sensitivity for the process $K^+ \to \mu^+ \nu_\mu X$, $X \to \gamma\gamma$ is evaluated, for masses m_X between 20 and 300 MeV/c^2. The best sensitivity is found to be of the order 10^{-7}, for m_X above 180 MeV/c^2.

Contents

1 Introduction

The anomalous magnetic moment of the muon has been measured experimentally and found to disagree with theoretical predictions by $\sim$3.5σ [1]. This discrepancy may be explained by a new type of particle arising in an extension to the Standard Model. One example of this is a light scalar particle X which couples to muons, and can act as a dark matter mediator [2]. In this report, the production of such a particle via the kaon decay $K^+ \to \mu^+ \nu_\mu X$ is investigated. The particle X may decay to two photons (via a muon loop), or to two muons for masses $m_X > 2m_\mu$. In this analysis only the photon decay mode is investigated.
Initially, a subset of NA62 data is analysed along with $K_{\mu 3}$ ($K^+ \to \mu^+ \nu_\mu \pi^0$) and $K_{2\pi}$ ($K^+ \to \pi^+ \pi^0$) MC samples. The $K_{\mu 3}$ decay is used as the signal, and a set of cuts is defined which selects the π^0 invariant mass peak. Next, the MC samples for the process $K^+ \to \mu^+ \nu_\mu X$, $X \to \gamma\gamma$ are analysed. A new set of cuts is defined, based on the previous selection, which selects this new signal. Finally, the NA62 BR sensitivity can be estimated for the production of X followed by a decay to two photons

2 Data and MC samples

The data used in this analysis were collected by NA62 in 2017 (run period 2017A). Data events are required to contain at least one good downstream track in the STRAW spectrometer and at least two unmatched clusters in the LKr calorimeter, and must pass the restricted muon filter. Monte Carlo samples have been produced for the $K_{\mu 3}$ and $K_{2\pi}$ processes, containing 5M and 50M events respectively. Recently produced MC signal samples are also used, for the process $K^+ \to \mu^+ \nu_\mu X$ followed by the prompt decay $X \to \gamma\gamma$. A range of masses m_X are considered, from 20 up to 380 MeV/c^2, increasing in steps of 20 MeV/c^2.

3 Preselection

A set of preselection crriteria is applied initially to select good quality events. The selection ResMuFilterAccepted = True ensures that events pass the restricted muon filter. Some events do not have measured values available for the kaon momentum from GTK beam spectrometer. In this case, the kaon momentum is set to $(p_x, p_y, p_z) = (0, 0, 75)$ GeV/c. Only events in which the kaon momentum is measured by GTK are selected. This is achieved by requiring a small, non-zero x-component of the kaon momentum ($60 < p_x < 120$ MeV/c). The distributions for the x, y and z components of the kaon momentum are shown in Fig. 1. These are plotted for NA62 data.

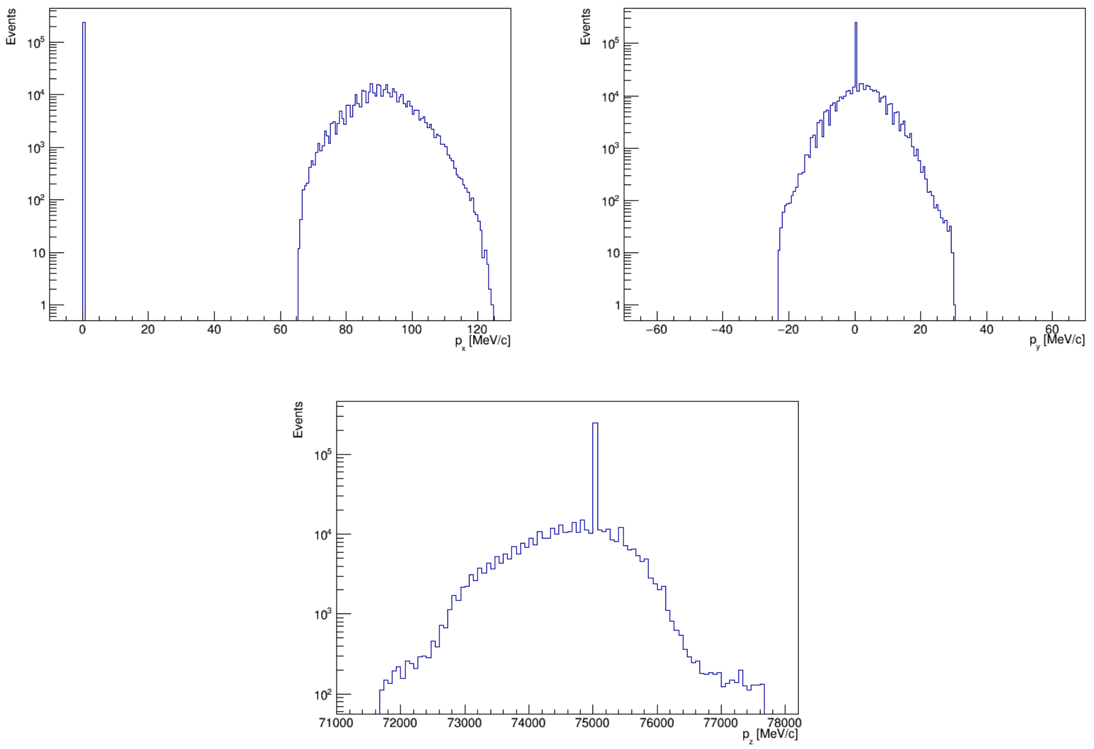

Figure 1: *Histograms for the x, y and z components of the kaon momentum for NA62 data, without any selection criteria applied. The distribution for the x-component shows a peak at around 90 MeV/c, representing events which have a measurement of the kaon momentum from GTK.*

An additional restriction on the kaon momentum, $72 < |\vec{p}(K^+)| < 78$ GeV/c , is also applied as part of preselection. Finally, it is required that the downstream track momentum $\vec{p}_{track}$ lies between 15 and 35 GeV/c. This ensures that information about particle identification obtained from the RICH detector is meaningful and can safely be used for identifying good muon candidates. Above 35 GeV/c, the RICH detector is ineffective at distinguishing between pions and muons. For momenta below 15 GeV/c, fewer Cerenkov photons are produced, leading to a lower efficiency for the RICH detector. The preselection criteria are summarised in Table 1.

Variable	Cut
ResMuFilterAccepted	True
$\vec{p}(K^+)$ measured by GTK	True
$\|\vec{p}(K^+)\|$	$72 < \|\vec{p}(K^+)\| < 78$ GeV/c
$\|\vec{p}_{track}\|$	$15 < \|\vec{p}_{track}\| < 35$ GeV/c

Table 1: *Preselection criteria. Events with measured values of kaon momentum (from GTK) are selected by requiring a small, non-zero x-component of kaon momentum.*

4 $K_{\mu 3}$ selection criteria

In this section, the $K_{\mu 3}$ MC sample is used as the signal. After applying preselection criteria additional cuts are used to select the π^0 peak in the $\gamma\gamma$ invariant mass distribution. These are described in Table 2. The signal signature is a single charged track (produced by a muon) along with two non-associated clusters in the LKr calorimeter (photons). Both of these requirements (nTrack = 1, nCluster = 2) are included in the set of $K_{\mu 3}$ selection criteria. The invariant mass of the two photons $m_{\gamma\gamma}$ is required to lie in the interval $110 < m_{\gamma\gamma} < 160$ MeV/c^2. This selects events with $\gamma\gamma$ invariant mass consistent with the π^0 mass. The 4-momenta of the two photons are determined assuming they originate from the $K^+ - \mu^+$ reconstructed vertex.

Variable	Cut	No of events		
		$K_{\mu 3}$	$K_{2\pi}$	Data
Preselection	True	759511	608483	9532096
$\lvert\vec{p}_{track} + \vec{p}_{\pi^0}\rvert$	<77 GeV/c	755728	600410	9353109
Good muon	True	715806	390602	6456727
nTrack	1	632599	390503	4893465
nCluster	2	384261	390490	2234080
$m_{\gamma\gamma}$	$110 < m_{\gamma\gamma} < 160$ MeV/c^2	379667	387107	2087674

Table 2: *$K_{\mu 3}$ selection criteria, applied to the NA62 data and $K_{\mu 3}$ and $K_{2\pi}$ MC samples after preselection. The numbers of data and MC events remaining after each cut are also listed. The 'good muon' variable includes several particle identification requirements.*

The variable called 'good muon' selects events in which the downstream particle is likely to be a muon. It takes into account several variables related to particle identification, from the RICH detector, the LKr calorimeter and the MUV3 muon detector. As well as requiring the muon probabilities to be close to 1, the electron and pion probabilities must be small for the good muon condition to be satisfied. The criteria are detailed in Table 3.

Variable	Cut
RICH most likely hypothesis	2
RICH probability (muon)	> 0.9
RICH probability (electron, pion)	< 0.5
Calorimeter probability (muon)	> 0.8
Calorimeter probability (electron, pion)	< 0.5
MUV3 association	True

Table 3: *Good muon selection criteria. RICH most likely hypothesis = 2 corresponds to a particle identified as a muon. The muon probabilities are required to be close to 1, and the electron and pion probabilities must be low for an event to pass the good muon selection.*

The distributions of some variables are shown after preselection and after all $K_{\mu 3}$ selection criteria are applied. The $\vec{p}_{track}$ distributions are plotted without applying the cut 15 $< |\vec{p}_{track}| <$ 35 GeV/c (Fig. 2). Some discrepancies can be seen between the data and MC distributions after preselection, particularly at high momentum, $\vec{p}_{track} >$ 40 GeV/c. However, the agreement is much better after the remaining cuts are applied. Any disagreement seen at high momentum is possibly due to the unreliability of the PID in this momentum range.

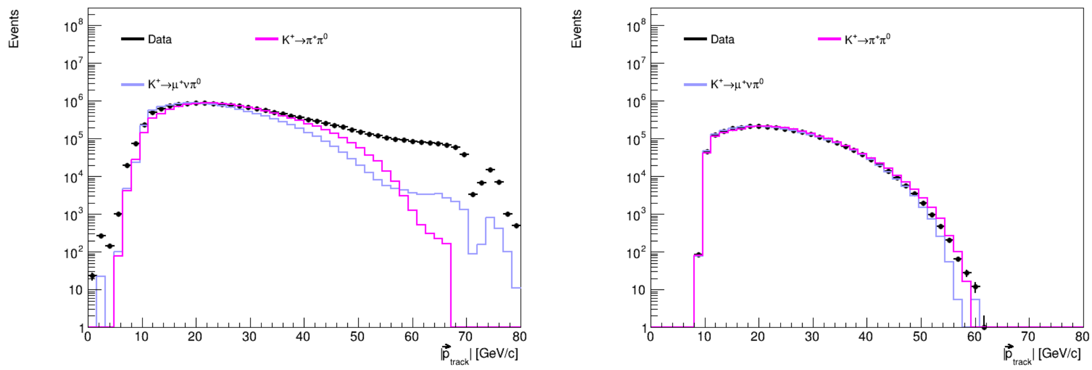

Figure 2: *Downstream track momentum $|\vec{p}_{track}|$, plotted (left) after preselection (excluding the cut on $|\vec{p}_{track}|$) and (right) after applying all cuts in Table 2 (excluding the cut on $|\vec{p}_{track}|$).*

The total momentum (sum of the track and π^0 momenta) is plotted in Fig. 3. The π^0 momentum is constructed from the momenta of the two photons. After all cuts are applied, the shape of the data distribution is in agreement with the $K_{\mu 3}$ distribution.

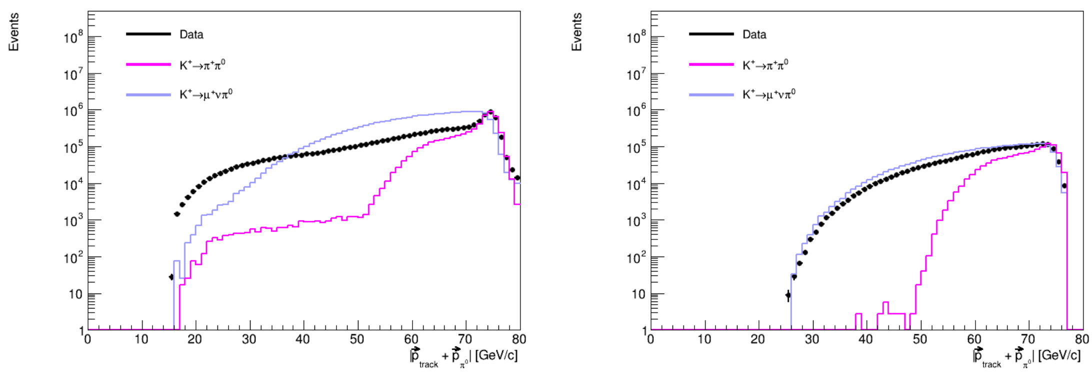

Figure 3: *Total momentum, $|\vec{p}_{track} + \vec{p}_{\pi^0}|$, plotted (left) after preselection and (right) after all cuts (excluding the cut on total momentum).*

The invariant mass of the two photons, $m_{\gamma\gamma}$, is plotted in Fig. 4, with a double-sided

CrystalBall function fitted to the π^0 mass peak since non-Gaussian tails are seen on both sides of the peak. The fit parameters are displayed: α_1 and n_1 are related to the tail on the left and α_2 and n_2 describe the tail on the right. A second smaller peak can also be seen close to zero.

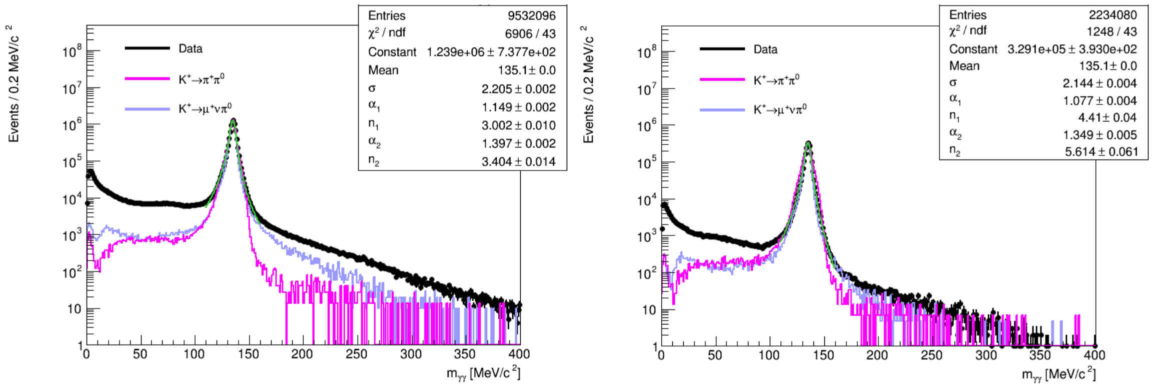

Figure 4: *Invariant mass of the two photons, $m_{\gamma\gamma}$, plotted (left) after preselection and (right) after all cuts (except for the cut on $m_{\gamma\gamma}$), for the $K_{\mu3}$ and $K_{2\pi}$ MC samples and NA62 data. A double-sided CrystalBall function is fitted to the π^0 mass peak in the data. The fitted function is shown in green.*

In Fig. 5 the total energy of the two photons, $E_{\gamma_1} + E_{\gamma_2}$, is shown (in this section this is equivalent to the π^0 energy). The $K_{2\pi}$ distribution is skewed towards higher values. Preselection requires that the downstream track momentum $\vec{p}_{track}$ lies between 15 and 35 GeV/c. For the two-body $K_{2\pi}$ decay, events with lower energy charged tracks will have a higher energy π^0, as seen in Fig. 5. The high energy tails seen in the data and the $K_{\mu3}$ MC after preselection are eliminated by the remaining cuts.

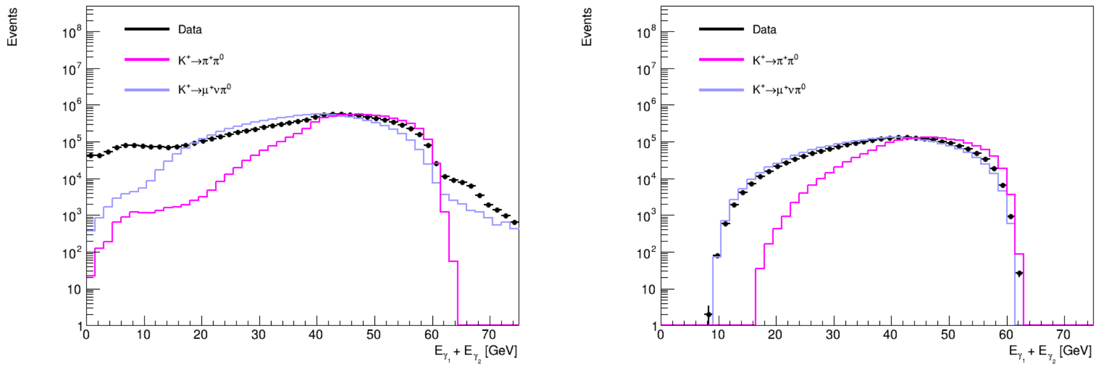

Figure 5: *Total cluster energy $E_{\gamma_1} + E_{\gamma_2}$, plotted (left) after preselection and (right) after all cuts. The $K_{2\pi}$ distribution is skewed towards higher energies.*

Additionally, a peak in the data is observed after preselection at around 10 GeV. This peak is inconsistent with the $K_{\mu3}$ and $K_{2\pi}$ MC, suggesting that there is another type of background present after preselection. This background may be $K_{\mu2}$ ($K^+ \to \mu^+\nu_\mu$). In this decay, there are no photons produced. The two non-asssociated clusters in the calorimeter are interpreted as accidental low-energy photons.

The low energy peak corresponds to events with low $\gamma\gamma$ invariant masses, which can be seen in Fig. 6. The plot on the left compares subsets of NA62 data. The $E_{\gamma_1} + E_{\gamma_2}$ distribution is plotted for events with $m_{\gamma\gamma} < 110$ MeV/c^2 and $110 < m_{\gamma\gamma} < 160$ MeV/c^2, with the distribution for the whole dataset shown on the same plot. At low energy, the shape of the low invariant mass distribution almost perfectly matches the overall distribution. At higher energies, the distribution for events with $m_{\gamma\gamma}$ consistent with the π^0 mass has a shape similar to that of the overall distribution.

The 2D histogram plotted on the right shows the correlation between the total cluster energy and $\gamma\gamma$ invariant mass. For events with $\gamma\gamma$ invariant mass consistent with the π^0 mass, the total cluster energy lies predominantly in the range 20 to 70 GeV. Events with low total cluster energy (< 10 GeV) tend to also have low $m_{\gamma\gamma}$. These events are therefore unlikely to contain a π^0.

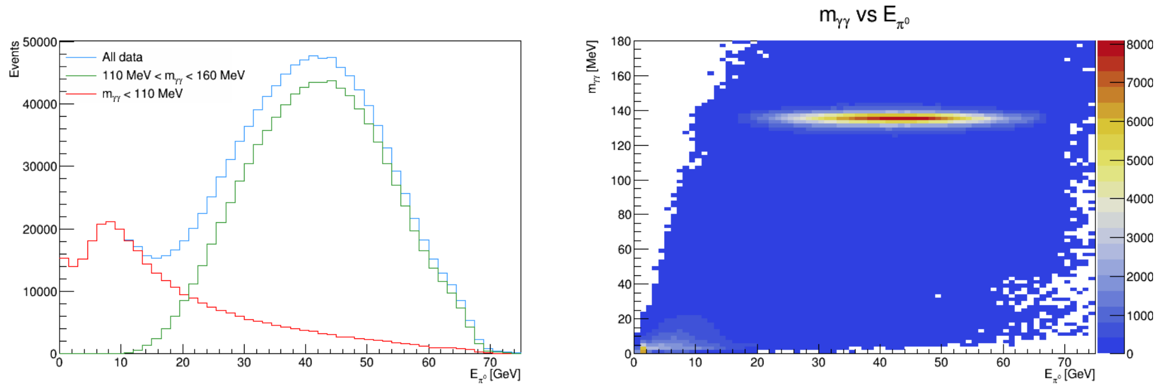

Figure 6: *Left: comparing total cluster energy ($E_{\gamma_1}+E_{\gamma_2}$) distributions for subsets of NA62 data. Distributions are plotted for events with $m_{\gamma\gamma} < 110$ MeV/c^2 (red) and $110 < m_{\gamma\gamma} < 160$ MeV/c^2 (green), with the distributions for the whole dataset shown in blue. Right: 2D histogram showing the correlation between the total cluster energy and $\gamma\gamma$ invariant mass.*

Finally, the distribution of the squared missing mass m^2_{miss} is plotted in Fig. 7. This variable is calculated using the 4-momenta of the kaon, the downstream track and the two photons, and assuming that the downstream particle is a muon:

$$m^2_{miss} = (P_K - P_\mu - P_{\gamma_1} - P_{\gamma_2})^2. \quad (1)$$

$K_{\mu3}$ events would be expected to have a squared missing mass consistent with zero, which can be seen on both plots. Before all cuts are applied, tails are observed in the data, lying above the tails in the MC distributions - some type of background besides $K_{\mu3}$ and $K_{2\pi}$ is probably present at this stage. After applying all further selection criteria, the tails are lowered, matching the MC more closely.

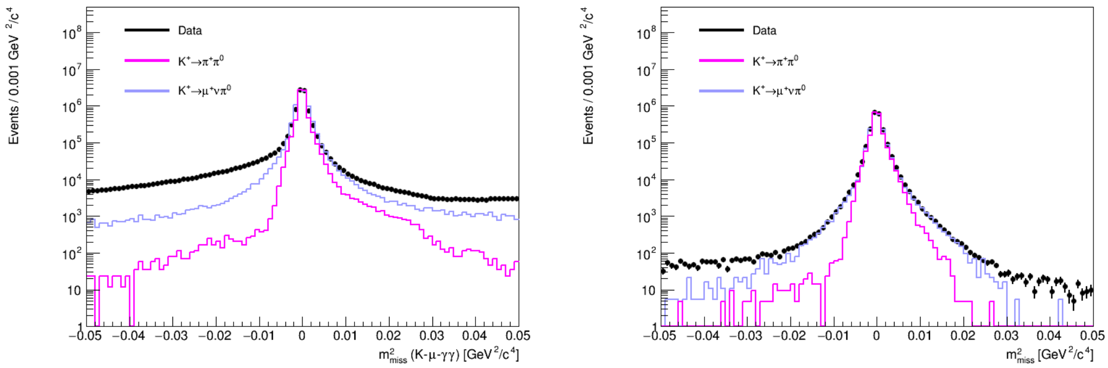

Figure 7: *Squared missing mass* $m^2_{miss} = (P_K - P_\mu - P_{\gamma_1} - P_{\gamma_2})^2$*, plotted (left) after preselection and (right) after all cuts. The squared missing mass peak is centered on zero as expected, for the NA62 data and both MC samples. After all selection criteria are applied, the shapes of the* m^2_{miss} *peaks for the NA62 data and* $K_{\mu 3}$ *MC match closely.*

In Fig. 8 the squared missing mass is plotted again, for subsets of the $K_{\mu 3}$ and $K_{2\pi}$ MC samples. These subsets contain events in which the kaon momentum is reconstructed (plotted in red) or is not reconstructed (plotted in blue). The missing mass calculation is carried out for a muon hypothesis (top two plots) and also assuming that the downstream particle is a pion (bottom two plots). A clear difference can be seen in the shapes of the two distributions (red and blue) in all cases, with narrower peaks observed for events in which the kaon momentum is reconstructed. The peaks are also offset from each other: the distributions for events without measured momentum values peak slightly below zero. Setting the kaon momentum to $(0, 0, 75)$ GeV/c instead of an average measured momentum value probably causes this offset. These plots illustrate the importance of selecting events which have GTK momentum measurements available.

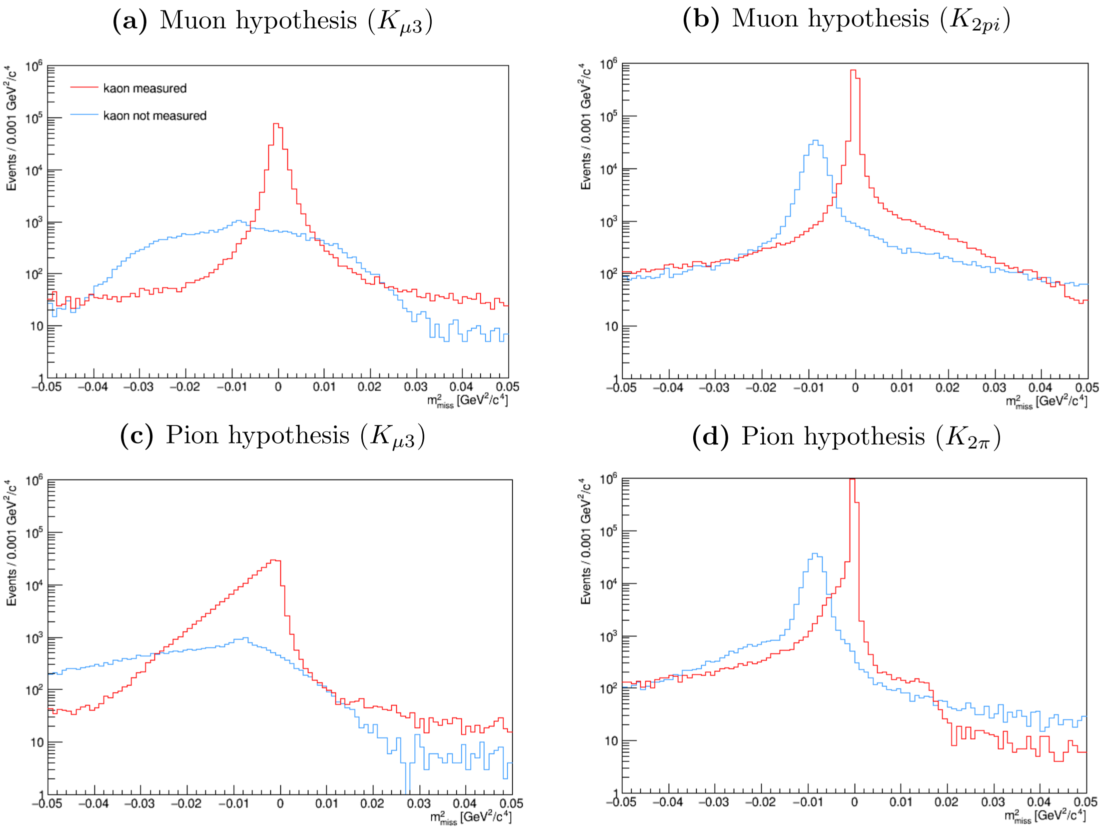

(a) Muon hypothesis ($K_{\mu 3}$)
(b) Muon hypothesis (K_{2pi})
(c) Pion hypothesis ($K_{\mu 3}$)
(d) Pion hypothesis ($K_{2\pi}$)

Figure 8: *Squared missing mass, $m^2_{miss} = (P_K - P_{track} - P_{\gamma_1} - P_{\gamma_2})^2$, plotted for subsets of the $K_{\mu 3}$ and $K_{2\pi}$ MC samples. In the top two plots the missing mass is calculated assuming that the downstream track is a muon, and the bottom two plots assume a pion hypothesis. Distributions are shown on the same plot for events in which the kaon momentum is measured by GTK (red) and events for which there is no kaon momentum measurement available (blue).*

5 Signal selection criteria

In this section, the $K_{\mu 3}$ sample is no longer used as the signal. Instead, MC samples for the production of the scalar particle X via the process $K^+ \to \mu^+ \nu_\mu X$ are used. The particle X decays promptly to two photons. There are 18 mass hypotheses included in the signal MC samples, starting from $m_X = 20$ MeV$/c^2$ and increasing in steps of 20 up to 360 MeV$/c^2$.
A new set of selection criteria is found, based on the cuts used in the previous section, but modified to select the new signal. These signal selection criteria are shown in Table 4. Most of the $K_{\mu 3}$ selection cuts used in Section 4 are also included here. The exception is the cut on $m_{\gamma\gamma}$, which is replaced by the final three criteria shown in blue. The additional cuts are applied to two different versions of the squared missing mass and to the total cluster energy.

Variable	Cut	No of events		
		$K_{\mu 3}$	$K_{2\pi}$	Data
Preselection	True	759511	608483	9532096
$\lvert\vec{p}_{track} + \vec{p}_{\pi^0}\rvert$	<77 GeV/c	755728	600410	9353109
Good muon	True	715806	390602	6456727
nTrack	1	632599	390503	4893465
nCluster	2	384261	390490	2234080
$m^2_{miss}(K-\mu)$	> 0.015 GeV$^2/c^4$	383898	390413	2126460
$m^2_{miss}(K-\mu-\gamma\gamma)$	-0.004 $< m^2_{miss} <$ 0.015 GeV$^2/c^4$	375815	386842	2066678
$E_{\gamma_1} + E_{\gamma_2}$	> 10 GeV	375785	386807	2064062

Table 4: *Signal selection criteria applied after preselection, and numbers of MC and data events left after each cut is applied. The selection criteria which differ from those in the previous section are shown in blue.*

Histograms are plotted below for some kinematic variables, after preselection and after all of the cuts in Table 4 are applied. Distributions are shown for the data and the $K_{\mu 3}$ and $K_{2\pi}$ MC samples, as well as two signal samples, with $m_X = 20$ and 280 MeV$/c^2$. The $K_{\mu 3}$ and $K_{2\pi}$ samples are scaled, with weights calculated in the following way:

- Find the numbers N_{obs} of $K_{\mu 3}$ and $K_{2\pi}$ observed MC events in the π^0 mass peak in the $m_{\gamma\gamma}$ distribution, after all signal selection criteria have been applied.
- Calculate efficiencies $\epsilon = \frac{N_{obs}}{N_{gen}}$ for both $K_{\mu 3}$ and $K_{2\pi}$ MC samples, where N_{gen} is the number of generated MC events.
- Find the normalised numbers of kaon decays $N_{norm} = \frac{N_{gen}}{BR}$ in both $K_{\mu 3}$ and $K_{2\pi}$ MC samples then normalise $K_{2\pi}$ MC sample to $K_{\mu 3}$ MC sample.
- Estimate the fractions of $K_{\mu 3}$ and $K_{2\pi}$ events in the π^0 mass peak, assuming that these are the only decays that contribute.

- Calculate the normalised number of kaon decays in NA62 data sample from the number of events observed in the π^0 mass peak.
- Find weights by normalising MC samples to the same normalised number of kaon decays as in NA62 data.

The signal samples shown in the plots are normalised to 1% of the data. The sample of $K_{2\pi}$ MC selected events is separated into events in which the π^+ decays in flight, and events in which the π^+ does not decay, and is misidentified as a muon. In the histograms plotted with all selection criteria applied, it can be seen that events with misidentified pions make up only a small fraction of $K_{2\pi}$ events. This suggets that the PID selection (good muon = True) works well and can accurately identify muons. The muons detected in $K_{2\pi}$ events originate from the decay $\pi^+ \to \mu^+\nu_\mu$.

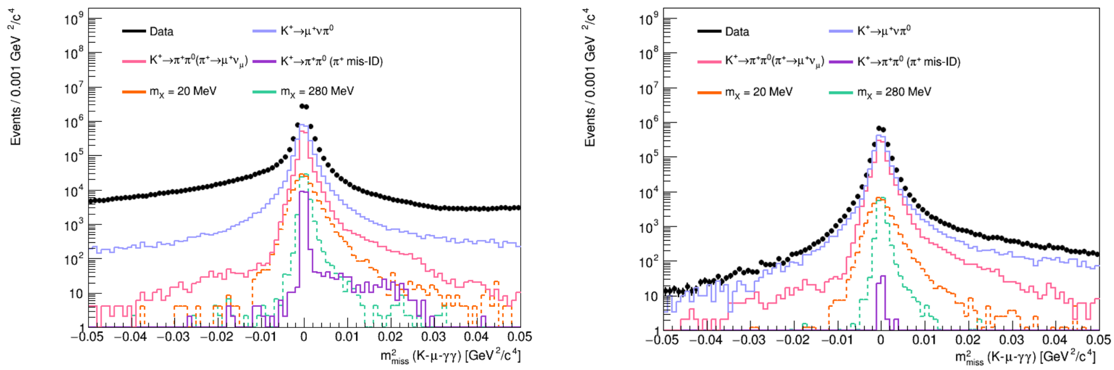

Figure 9: *Squared missing mass $m^2_{miss}(K-\mu-\gamma\gamma) = (P_K - P_\mu - P_{\gamma_1} - P_{\gamma_2})^2$, plotted after preselection (left), and after applying all signal selection criteria except the cut on $m^2_{miss}(K-\mu-\gamma\gamma)$ (right). After preselection, the tails in the data lie above the MC distributions. After further cuts, the agreement between data and $K_{\mu3}$ MC is much better.*

The variable $m^2_{miss}(K-\mu-\gamma\gamma) = (P_K - P_\mu - P_{\gamma_1} - P_{\gamma_2})^2$ is plotted in Fig. 9: (left) after preselection and (right) after all cuts except the one on $m^2_{miss}(K-\mu-\gamma\gamma)$. The tails in the data distribution are lowered after the full set of signal selection criteria is applied, so that the shape matches the $K_{\mu3}$ distribution more closely. Any component in the data due to decays other than $K_{\mu3}$ and $K_{2\pi}$ appears to be removed by the final cuts. The cut on $m^2_{miss}(K-\mu-\gamma\gamma)$ selects events lying within the peak, cutting out any remaining events in the tails of the distribution.
The missing mass $m^2_{miss}(K-\mu) = (P_K - P_\mu)^2$ is shown in Fig. 10. In the second histogram, all cuts are applied except for the cut on $m^2_{miss}(K-\mu)$. A sharp peak centered on zero is seen in the data, with a similarly shaped peak in the same place for the $K_{\mu3}$ distribution. The $K_{\mu3}$ peak is much smaller than the peak in data, suggesting that a different type of background, potentially $K_{\mu2}$, also contributes. This type of decay is

expected to have a $(K - \mu)$ missing mass consistent with zero. The set of signal selection criteria includes a requirement that this squared missing mass is greater than 0.015 GeV^2/c^4, which eliminates the peak at zero and should cut out $K_{\mu 2}$ events. A second peak at $m^2_{miss}(K - \mu) \simeq 0.03\ \mathrm{GeV}^2/c^4$ is also seen in the data, and matches the shape of the $K_{2\pi}$ distribution. The size of this peak is reduced after all cuts are applied, in both the $K_{2\pi}$ and the data distributions.

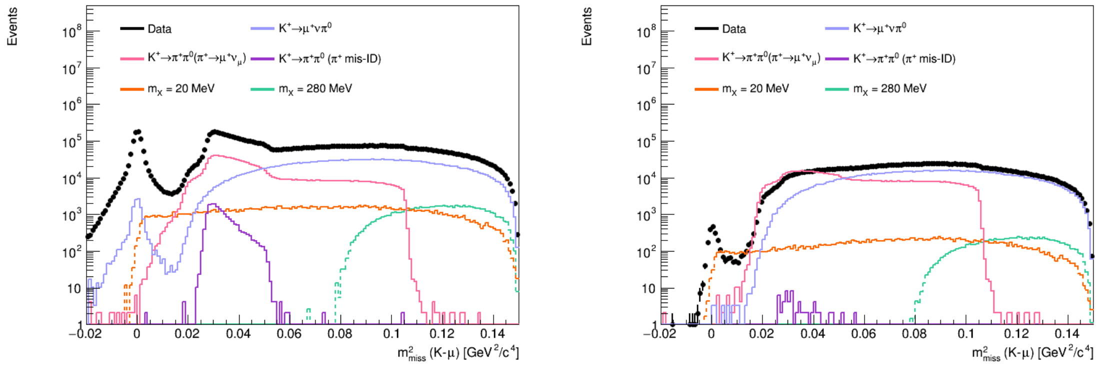

Figure 10: *Squared missing mass $m^2_{miss} = (P_K - P_\mu)^2$, plotted after preselection (left), and after applying all signal selection criteria except the cut on $m^2_{miss}(K - \mu)$ (right). After preselection, a peak centered on zero is seen in the data, which may be partially due to $K_{\mu 2}$ events. A peak in the data is also seen above zero, this disappears after further cuts are applied.*

Two additional variants on the squared missing mass are considered, both calculated assuming that the downstream particle is a pion. The $(K - \pi - \gamma\gamma)$ squared missing mass distribution, plotted in Fig. 11, has a similar shape for the signal and background MC samples and the NA62 data, so no cuts are made on this variable. The final squared missing mass variable, $m^2_{miss}(K - \pi) = (P_K - P_\pi)^2$, is plotted in Fig. 12. After preselection, a peak is seen in the data just below zero, matching the shape of the $K_{\mu 3}$ distribution. A peak is also seen above zero, mostly due to $K_{2\pi}$ events. The first peak is removed by the signal selection criteria. The second peak, although it is reduced in size, is still visible. If further work is carried out to refine the selection criteria, this may be a useful variable to consider.

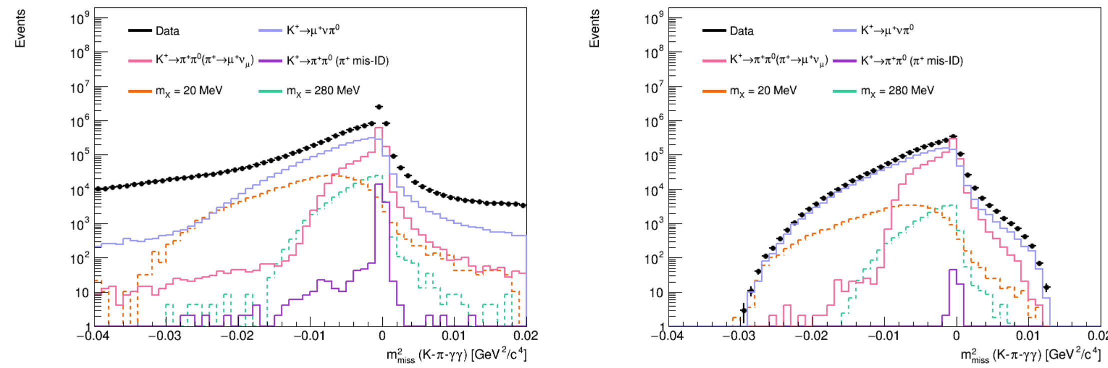

Figure 11: *Squared missing mass* $m^2_{miss} = (P_K - P_\pi - P_{\gamma 1} - P_{\gamma 2})^2$*, plotted after preselection (left), and after applying all selection criteria in Table 4 (right). The tails in the data lie above the MC distributions after preselection. These tails are lowered after all cuts are applied, giving good agreement between data and* $K_{\mu 3}$ *MC.*

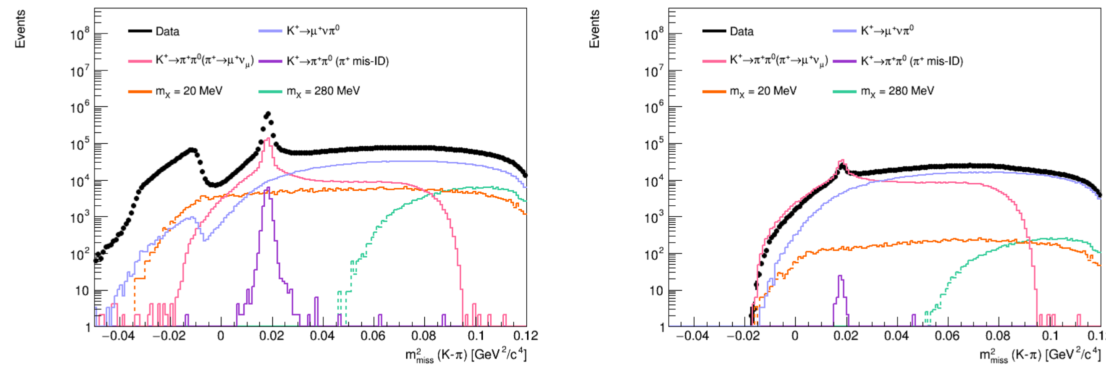

Figure 12: *Squared missing mass* $m^2_{miss} = (P_K - P_\pi)^2$*, plotted after preselection (left), and after applying all selection criteria in Table 4 (right). The peaks at negative* m^2_{miss} *seen in the data and* $K_{\mu 3}$ *distributions are removed by the final cuts. A peak at positive* m^2_{miss} *is seen in the data and* $K_{2\pi}$ *after preselection. This peak is reduced in size by signal selectins but is still present.*

The missing momentum $\vec{p}_{miss}$ is given by the difference between the 3-momenta of the kaon, and the muon and two photons: $\vec{p}_{miss} = \vec{p}_K - \vec{p}_\mu - \vec{p}_{\gamma_1} - \vec{p}_{\gamma_2}$. The missing transverse momentum $\vec{p}_{T,miss}$ is the component of the missing momentum perpendicular to the kaon direction of flight. The average values for the components of the kaon momentum are taken from the events in NA62 data which have the kaon momentum measured by GTK. By construction $\vec{p}_{miss}$ and $\vec{p}_{T,miss}$ do not depend on mass hypothesis for the charged particle. These values give the kaon direction of flight used to calculate $\vec{p}_{T,miss}$. The distributions for both of these variables (Fig. 13) show high momentum tails in the data and $K_{\mu 3}$, and also peaks at very low momentum in the data and $K_{2\pi}$. Both of these features are reduced or removed by the signal selection criteria.

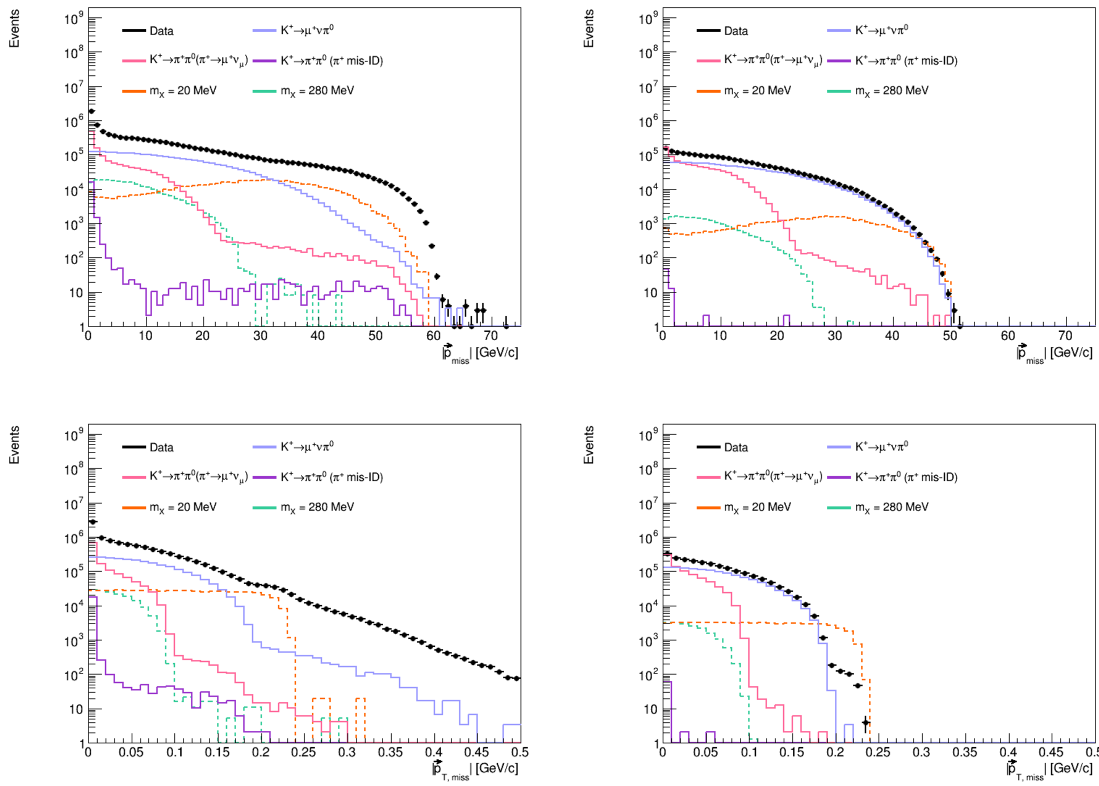

Figure 13: *Top: missing momentum $|\vec{p}_{miss}|$, plotted after preselection (left), and after applying all selection criteria in Table 4 (right). Bottom: missing transverse momentum $|\vec{p}_{T,miss}|$, plotted after preselection (left), and after applying all selection criteria in Table 4 (right).*

6 Calculating branching ratio sensitivity

With the signal selection criteria applied, the branching ratio sensitivity can be calculated. A search region $m_X \pm N_\sigma^{int}\sigma(m_X)$ is defined, where $\sigma(m_X)$ is the width of the $\gamma\gamma$ invariant mass peak (measured on signal MC) as a function of m_X, and N_σ^{int} is chosen to be 2. Assuming a large background in the search interval, the number of background events in this interval is $N_B = 2N_\sigma^{int}\sigma(m_X)f_1(m_X)$. The function $f_1(m_X)$ describes the shape of the $m_{\gamma\gamma}$ background distribution. The number of signal events in the search interval is $N_S = N_{norm}BR\epsilon_S$, where N_{norm} is the normalised number of kaon decays, corresponding to the total number of kaon decays in the fiducial volume divided by the trigger downscaling factor, in the NA62 data sample, and ϵ_S is the signal efficiency (fraction of signal events in the search region remaining after all signal selection criteria are applied). A significance $N_\sigma^{sign} = 5$ is chosen, and the discovery condition is $\frac{N_S}{\sqrt{N_B}} > N_\sigma^{sign}$. An expression for the BR sensitivity as a function of m_X and N_{norm} is then obtained as the BR value for which $\frac{N_S}{\sqrt{N_B}} = N_\sigma^{sign}$ is satisfied:

$$BR\ sensitivity(m_X, N_{norm}) = \frac{N_\sigma^{sign}\sqrt{2N_\sigma^{int}\sigma(m_X)f_1(m_X)}}{\epsilon(m_X)N_{norm}} \tag{2}$$

The signal efficiency ϵ_S is calculated for each value of m_X using the signal MC sample and plotted in Fig. 14. A 2nd order polynomial is fitted to these points, and the function obtained is:

$$\epsilon_S(m_X) = 0.2566 + 1.996\times10^{-3}\frac{m_X}{MeV/c^2} - 4.353\times10^{-6}\frac{m_X^2}{MeV^2/c^4}. \tag{3}$$

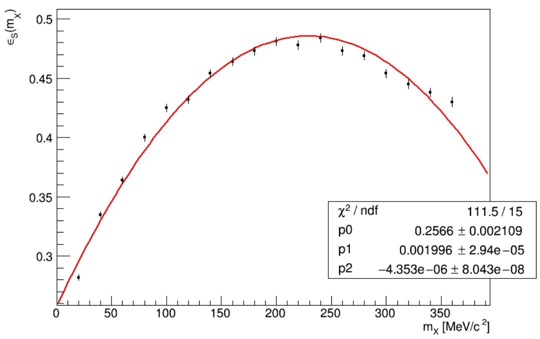

Figure 14: *Signal efficiency ϵ_S as a function of m_X. Points fitted with 2nd order polynomial.*

For each generated m_X value in the signal MC sample the $\gamma\gamma$ invariant mass peak is plotted and fitted with a double-sided CrystalBall function. This function with a tail on both sides of the peak is found to fit the distribution better than a CrystalBall function

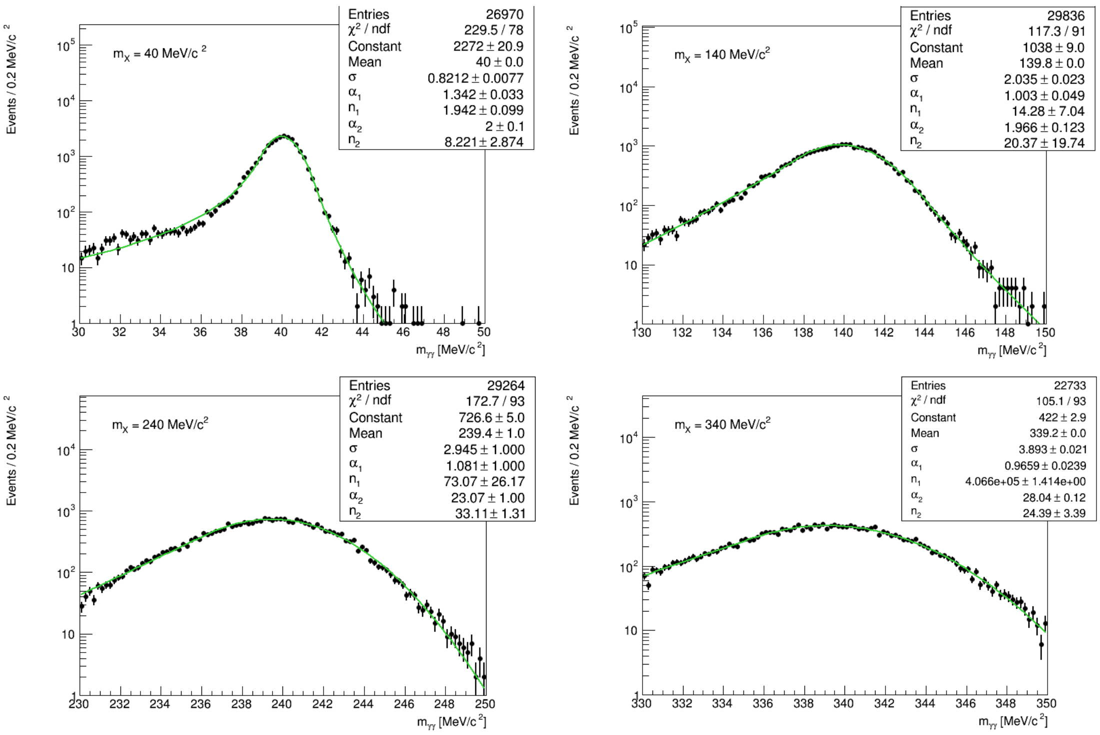

Figure 15: *$m_{\gamma\gamma}$ distribution showing the signal invariant mass peak for four mass hypotheses: $m_X = 40, 140, 240, 340$ MeV/c^2. Each peak is fitted with a double-sided CrystalBall function (green), with the fit parameters displayed.*

with a tail on only one side. Some of these plots are shown in Fig. 15. The points represent the signal MC and the green lines are the fitted CrystalBall functions. From these fits, values are obtained for the peak width σ for each m_X value. This is plotted in Fig. 16 with a 1st order polynomial fitted:

$$\sigma(m_X) = 0.3904 + 0.01057\frac{m_X}{MeV/c^2}. \tag{4}$$

The final requirement for calculating the BR sensitivity is a function $f_1(m_X)$ describing the $m_{\gamma\gamma}$ background. This function is found by fitting the $m_{\gamma\gamma}$ distribution for the NA62 data. It is found that a double-sided CrystalBall function works well for describing the π^0 mass peak, however the fit is not as good for the regions outside of the peak. A better fit is achieved by defining a function which is the sum of a CrystalBall function $C(m_X)$ and a fourth order polynomial $p(m_X)$. The functions obtained from the fit are given in eq. (5) and eq. (6).

$$p(m_X) = 215.6 - 2.393\frac{m_X}{MeV/c^2} + 8.885\times10^{-3}\frac{m_X^2}{MeV^2/c^4} - 1.096\times10^{-5}\frac{m_X^3}{MeV^3/c^6}, \tag{5}$$

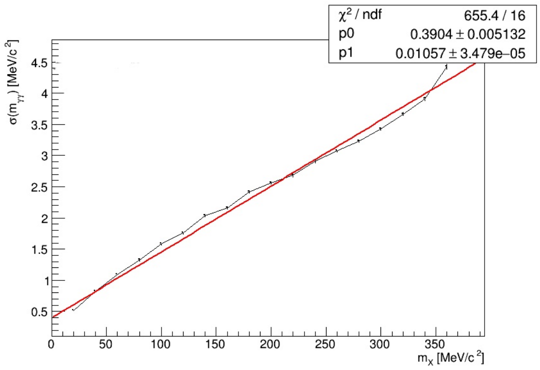

Figure 16: *Signal peak width σ as a function of m_X. Points fitted with 1st order polynomial.*

$$C(m_X) = \begin{cases} 1.861 \times 10^5 \Big(64.16 - \dfrac{m_X}{2.131}\Big)^{-4.743} & m_X < 132.8 \\ 3.278 \times 10^5 \exp\Big(-\dfrac{1}{2}\Big(\dfrac{m_X - 135.1}{2.131}\Big)^2\Big) & 132.8 < m_X < 138.0 \\ 1.272 \times 10^5 \Big(\dfrac{m_X}{2.131} - 62.63\Big)^{-8.055} & m_X > 138.0 \end{cases} \quad (6)$$

The overall background function is the sum, $f_1(m_X) = C(m_X) + p(m_X)$. The $m_{\gamma\gamma}$ distribution is plotted in Fig. 17 for the NA62 data, with the fitted function $f_1(m_X)$ shown in green.

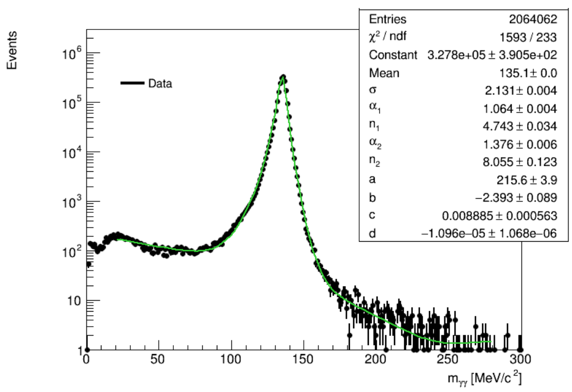

Figure 17: *$m_{\gamma\gamma}$ distribution for NA62 data, fitted with the sum of a double-sided Crystal-Ball function and a 4th order polynomial.*

Using the fitted functions described above, the BR sensitivity can be plotted as a function of m_X. This is shown in Fig. 18. There is very little sensitivity in the range $100 < m_X < 160$ MeV/c^2 due to the π^0 mass peak from $K_{\mu 3}$ irreducible background. For lower values of m_X the BR sensitivity is of the order 10^{-6}, while for the higher m_X values, BR sensitivity of order 10^{-7} is estimated.

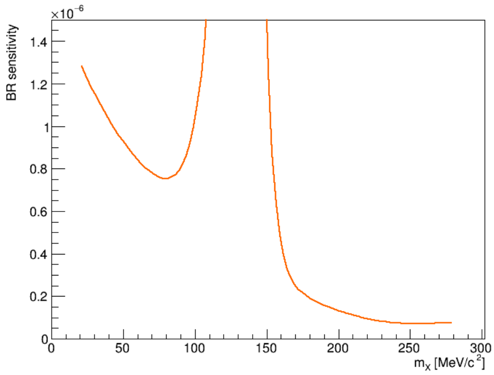

Figure 18: *BR sensitivity for the decay $K^+ \to \mu^+\nu_\mu X$, $X \to \gamma\gamma$ as a function of m_X.*

The data sample used in this analysis, from run period 2017A, corresponds to (5.0±0.5) % of the NA62 Run 1 statistics. BR sensitivity scales as $\frac{1}{\sqrt{N(K\ decays)}}$. Extrapolating to the full NA62 Run 1 statistics would therefore be expected to improve the sensitivity by a factor of ∼4.5.

7 Conclusions

A first estimate is found for the NA62 sensitivity to the rare decay $K^+ \to \mu^+\nu_\mu X$, $X \to \gamma\gamma$. A range of mass hypotheses are considered, for m_X between 20 and 300 MeV/c^2. The best sensitivity, of order 10^{-7}, is achieved for higher values of m_X. The sensitivity is estimated for the full 2017A dataset collected by NA62, which makes up (5.0±0.5) % of the total Run 1 statistics. With the whole Run 1 dataset, the sensitivity would be expected to improve by a factor of ∼4.5. For further work on this decay, the selection criteria could be refined further. Additional components are seen in the data distributions that are not accounted for by $K_{\mu3}$ and $K_{2\pi}$ decays. This could be further investigated, for example by simulating $K_{\mu2}$ events which could account for some of this background.

Acknowledgements

I would like to thank my tutors, A. Bizzeti and D. Redigolo, and also F. Bucci, for their help and guidance throuhgout this project. I would also like to thank the NA62 Collaboration for allowing me to access NA62 data.

References

[1] G. W. Bennett *et al.* (Muon g-2 Collaboration), Phys. Rev. D **73** (2006), 072003 [arXiv:hep-ex/0602035 [hep-ex]].

[2] G. Krnjaic, G. Marques-Tavares, D. Redigolo and K. Tobioka, Phys. Rev. Lett. **124** (2020) no.4, 041802 [arXiv:1902.07715 [hep-ph]].